Clinical Cancer Research

Immunotherapeutic Blockade of Macrophage Clever-1 Reactivates the CD8$^+$ T-cell Response against Immunosuppressive Tumors

Miro Viitala[1,2], Reetta Virtakoivu[1], Sina Tadayon[1,2], Jenna Rannikko[1], Sirpa Jalkanen[1], and Maija Hollmén[1]

Abstract

Purpose: As foremost regulators of cancer-related inflammation and immunotherapeutic resistance, tumor-associated macrophages have garnered major interest as immunotherapeutic drug targets. However, depletory strategies have yielded little benefit in clinical studies to date. An alternative approach is to exploit macrophage plasticity and "reeducate" tumorigenic macrophages toward an immunostimulatory phenotype to activate the host's antitumor immunity.

Experimental Design: We investigated the role of the macrophage scavenger receptor common lymphatic endothelial and vascular endothelial receptor-1 (Clever-1) on tumor growth in multiple mouse cancer models with inflammatory and noninflammatory characteristics by using conditional knockouts, bone marrow chimeras, and cell depletion experiments. In addition, the efficacy of immunotherapeutic Clever-1 blockade as monotherapy or in combination with anti-PD-1 was tested.

Results: Genetic deficiency of macrophage Clever-1 markedly impaired solid tumor growth. This effect was mediated by macrophages that became immunostimulatory in the absence of Clever-1, skewing the suppressive tumor microenvironment toward inflammation and activating endogenous antitumor CD8$^+$ T cells. Comparable effects were achieved with immunotherapeutic blockade of Clever-1. Notably, these effects were similar to those achieved by PD-1 checkpoint inhibition. Moreover, combining anti-Clever-1 with anti-PD-1 provided synergistic benefit in aggressive, nonresponsive tumors.

Conclusions: These findings demonstrate the importance of macrophages in mediating antitumor immune responses and support the clinical evaluation of immunotherapeutic Clever-1 blockade as a novel cancer treatment strategy.

See related commentary by Mantovani and Bonecchi, p. 3202

Introduction

Cancer immunotherapy has proven effective for a wide range of human malignancies, but solely for the minority of patients (1). Efficient and durable immunotherapies require adaptive immune activation, namely antitumor CD8$^+$ T cells (2). On the basis of immune cells infiltrating the tumor microenvironment (TME), tumors have been categorized into two main immunologic phenotypes: inflamed tumors with spontaneous immune cell infiltration and noninflamed tumors that lack a noticeable antitumor immune response (3). Preselection of patients is essential to achieve therapeutic outcomes, because only a minority of unselected patients benefit from checkpoint blockade. For example, inhibiting PD-1/PD-L1 interaction in inflamed tumors can reactivate CD8$^+$ T cells in the TME, sometimes leading to dramatic tumor regression, whereas noninflamed tumors are typically refractory to immune checkpoint blockade (4). Still, not even all inflamed tumors respond to anti-PD-1/PD-L1 immunotherapies, and patients with an initial response may develop resistance. Thus, novel, alternative approaches are required to reactivate antitumor immunity in a wider range of patients to overcome immunotherapeutic resistance in both inflamed and noninflamed tumor types (5).

Macrophages are highly adaptable cells that can either stimulate or suppress the immune system depending on environmental cues. Tumor-associated macrophages (TAM) and myeloid-derived suppressor cells (MDSC) are foremost regulators of cancer-related inflammation, cancer progression, and immunotherapeutic resistance (6). Mirroring classical M1 and alternative M2 macrophage activation, TAMs tend to acquire an M2-like tumorigenic phenotype that promotes cancer progression in a multitude of ways. However, despite some success in preclinical models, immunotherapies that rely on the complete depletion of TAMs have not shown great success in clinical trials to date. Exploiting the inherent plasticity of macrophages has been suggested as an alternative approach, and the concept of reeducating tumorigenic TAMs to acquire an immunostimulatory phenotype has been proven in multiple mouse models. Novel strategies for specifically depleting or converting tumorigenic TAMs are therefore actively sought in immuno-oncological research (6).

Common lymphatic endothelial and vascular endothelial receptor-1 (Clever-1)—encoded by the *Stab1* gene and also called Stabilin-1 or Feel-1—is a conserved, multifunctional adhesion and scavenger receptor expressed by subsets of endothelial cells,

[1]MediCity Research Laboratory, Institute of Biomedicine, Faculty of Medicine, University of Turku, Turku, Finland. [2]Turku Doctoral Program of Molecular Medicine, University of Turku, Turku, Finland.

Note: Supplementary data for this article are available at Clinical Cancer Research Online (http://clincancerres.aacrjournals.org/).

Corresponding Author: Maija Hollmén, University of Turku, Tykistökatu 6A 4th Floor, Turku, District of South-Western Finland 20520, Finland. Phone: 358-5051-42893; E-mail: maija.hollmen@utu.fi

Clin Cancer Res 2019;25:3289–303

doi: 10.1158/1078-0432.CCR-18-3016

Translational Relevance

Overcoming cancer-related immunosuppression presents a significant obstacle to successful treatment. We report macrophage repolarization by immunotherapeutic Clever-1 blockade as an alternative to checkpoint blockade to reactivate antitumor immunity against immunosuppressive tumors.

immunosuppressive macrophages, and TAMs (7–11). Clever-1 mediates cell adhesion and the scavenging and intracellular trafficking of its ligands (7, 12–16). Recent reports by us and others indicate that Clever-1 also advantages tumor progression (8–10, 17). However, the proposed tumorigenic mechanisms center on the paradigm of Clever-1 as an adhesion and scavenger receptor and do not explain the direct immunosuppressive functions of Clever-1$^+$ monocytes and macrophages we have recently described (11, 18, 19). Mechanistic details explaining how macrophage Clever-1 regulates innate–adaptive immune crosstalk and cancer-related inflammation are not fully understood.

Here, our objective was to elucidate how macrophage Clever-1 regulates antitumor immunity. We found that the growth of multiple solid tumor models is significantly impaired when Clever-1 is removed specifically from macrophages. With bone marrow chimeras and cell depletion experiments, we could identify macrophages deficient of Clever-1 as the initiators of antitumor immunity. Lack of Clever-1 in macrophages associated with an increasingly immunostimulatory phenotype and enhanced signaling through the inflammatory mTOR pathway. Finally, we demonstrated that immunotherapeutic Clever-1 blockade can reactivate the antitumor CD8$^+$ T-cell response, with comparable therapeutic responses to PD-1 checkpoint blockade.

Materials and Methods

Cell lines

The LLC1 Lewis lung carcinoma, E0771 medullary mammary adenocarcinoma, and EL4 lymphoma cell lines were cultured in complete DMEM (Sigma-Aldrich; DMEM supplemented with 10% FCS and penicillin/streptomycin). The 4T1-luc2 mammary gland carcinoma and CT26.WT colon carcinoma were cultured in complete RPMI1640 (Sigma-Aldrich; RPMI1640 supplemented with 10% FCS, 2 mmol/L L-glutamine, 1 mmol/L sodium pyruvate, and penicillin/streptomycin). The LLC1, EL4, and CT26.WT cell lines were obtained from ATCC. The 4T1-luc2 cell line was obtained from Caliper Life Sciences. The E0771 cell line was a generous gift from Prof. Burkhard Becher (University of Zürich, Zurich, Switzerland). The cell lines were routinely tested for *Mycoplasma*. Cell line authentication was not routinely performed.

Mouse models and therapeutic treatments

All animal experiments were performed in adherence to the Finnish Act on Animal Experimentation (62/2006) and were approved by the Committee for Animal Experimentation (license numbers 5587/04.10.07/2014 and 5762/04.10.07/2017). Mice were used at 2 to 4 months of age. Experimental groups were matched for age and sex. The full and conditional Clever-1 knockout mouse strains and their wild-type controls are from the C57BL/6N:129SvJ mixed background and were generated as described previously (10). To generate reporter mice, Tg (CAG-DsRed*MST)1Nagy/J mice were purchased from Jackson Laboratories and crossbred with Clever-1 knockout mice to generate DsRed and DsRed/Clever-1$^{-/-}$ reporter strains. To generate LLC1, EL4 or CT26.WT tumors, 0.5×10^6 cells in 200 μL of PBS were injected subcutaneously into the flanks. To generate orthotopic E0771 or 4T1-luc2 tumors, 0.1×10^6 cells in 50 μL of PBS were injected subcutaneously into the fourth mammary fat pads. Tumor outgrowth was measured with digital calipers. The humane endpoint for tumor diameter was 15 mm. Tumor volumes were calculated as follows: longer diameter × shorter diameter^2/2. To generate bone marrow chimeras, wild-type recipients were irradiated twice with 5 Gy with a 3-hour interval and injected intravenously with 1×10^7 bone marrow cells from DsRed or DsRed/Clever-1$^{-/-}$ reporter mice. Mice were allowed to reconstitute for 2 months before being used for experiments. Chimerism was determined by measuring the frequency of DsRed$^+$ cells in the blood. To deplete macrophages or CD8$^+$ T cells, mice received 200 μg of anti-CD115 (AFS98; BioXCell) every other day or 100 μg of anti-CD8β (53-5.8; BioXCell) once weekly, respectively, or a combination of equivalent amounts of irrelevant IgGs (2A3 and HRPN, respectively; BioXCell) intraperitoneally in PBS from 8 days before the cancer cell injection until endpoint. For immunotherapy, tumor-bearing mice received 200 μg of anti-Clever-1 [mStab1-1.26 (mouse IgG1), InVivo Biotech; 20], 200 μg of anti-PD-1 (RMP1-14; BioXCell), or a combination of equivalent amounts of irrelevant IgGs (MOPC-21 and 2A3, respectively; BioXCell) intraperitoneally in PBS on days 3, 6, 9, and 12 after cancer cell injection.

Ex vivo bioluminescence imaging

On the day of sacrifice, mice received 150 mg/kg of D-luciferin substrate intraperitoneally (Caliper Life Sciences) and were sacrificed after 5 minutes by CO_2 asphyxiation. The lungs and lymph nodes were excised and imaged with the IVIS system after 10 minutes with the following settings: exposure time = 10 seconds (lungs) or 30 seconds (lymph nodes), f/stop = 1, medium binning, field of view = 3.9 × 3.9 cm^2. Living Image software was used to quantify the bioluminescent signal reported as units of tissue radiance (photons/s/cm^2/sr).

Flow cytometric analysis

Mice were sacrificed by CO_2 asphyxiation. Lymph nodes were dissociated mechanically. Tumors were processed into single-cell suspensions with the Mouse Tumor Dissociation Kit per manufacturer's instructions (130-096-730; Miltenyi Biotec) and passed through 70 μm pre-separation filters (130-095-823; Miltenyi Biotec). Myeloid cells and T cells were enriched sequentially with CD11b and CD90.2 Microbeads, respectively (130-049-601 and 130-049-101; Miltenyi Biotec) on MS columns (130-042-201; Miltenyi Biotec). Cells were labeled with a fixable viability dye (eFluor 450 or eFluor 780; Invitrogen) and stained with conjugated primary antibodies against mouse CD3 (17A2; BD Biosciences), CD4 (GK1.5; BioLegend), CD8α (53-6.7; BD Biosciences), CD11b (M1/70; BD Biosciences), CD45 (30-F11; BD Biosciences), CD206 (C068C2; BioLegend), Ly6C (AL-21; ThermoFisher Scientific), Ly6G (BD Biosciences), FoxP3 (Thermo Fisher Scientific), Ki67 (SolA15; Thermo Fisher Scientific), Lag3 (ThermoFisher Scientific), Nos2 (CXNFT; ThermoFisher Scientific), and PD-1 (Thermo Fisher Scientific), or an irrelevant IgG control antibody with Fc block (2.4G2; BD Biosciences). Anti-

Clever-1 (mStab1-1.26; InVivo Biotech) and its irrelevant IgG control antibody (MOPC-21; BioXCell) were conjugated with the Alexa Fluor 647 Protein Labeling Kit (A20173; Invitrogen). Cells were fixed with 4% paraformaldehyde (sc-281692; Santa Cruz Biotechnology) and stained in 1× Permeabilization Buffer (00-8333-56; Thermo Fisher Scientific) to detect intracellular antigens (Clever-1, CD206, Nos2). The Transcription Factor Staining Buffer Set (00-5523-00; Invitrogen) was used for simultaneous detection of cell-surface and intranuclear antigens (Ki67, FoxP3). Samples were acquired with LSRFortessa (BD Biosciences) and analyzed with FlowJo 10 (TreeStar). Cell numbers per mg of tumor were calculated as follows: number of acquired events/acquired volume × sample volume/tumor weight.

IHC

For hematoxylin/eosin staining, 5-μm–thick tumor sections were stained with ready-to-use hematoxylin (CS700), Bluing Solution (CS702), and eosin (CS701) from Dako. Briefly, sections were washed with Milli-Q water, stained with hematoxylin, and washed again with Milli-Q water and 70% ethanol. Next, sections were incubated with Bluing Solution, washed with Milli-Q water and ethanol, stained with eosin, and washed with ethanol and xylene before mounting with DPX Mountant (06522; Sigma Aldrich). Samples were imaged with a Panoramic 250 Slide Scanner (3D Histech Ltd.). For immunofluorescence staining, 5-μm–thick tumor sections were fixed and permeabilized with acetone. Sections were stained with anti-mouse CD3 (ab33429; Abcam), CD31 (550274; BD Biosciences), F4/80 (53-4801-82; Thermo Fisher Scientific), and Clever-1 (9-11; InVivo Biotech) or an irrelevant IgG control antibody. Sections were washed with PBS and the nuclei were stained with Hoechst. Sections were mounted with Vectashield Mounting Medium. Images were acquired with a Carl Zeiss LSM780 laser scanning confocal microscope. The anti-Clever-1 antibody 9-11 was conjugated with the Alexa Fluor 647 Protein Labeling Kit as described above.

Enrichment of TAMs and MDSCs

Tumors were processed into single-cell suspensions as described above. First, monocytic (M)-MDSCs and polymorphonuclear (PMN)-MDSCs were enriched as one pool with the Myeloid-derived Suppressor Cell Isolation Kit (130-094-538; Miltenyi Biotec), after which TAMs were enriched from the negative fraction with CD11b Microbeads. The purity of enriched MDSCs was over 90% (live $CD11b^{+}$ $Ly6C^{intermediate}$ $Gr\text{-}1^{+}$). The remaining CD11b fraction contained TAMs ($Ly6C^{low}$ $Gr\text{-}1^{-}$) and some $Ly6C^{high}$ monocytes.

Generation of bone marrow–derived macrophages

Wild-type and Clever-$1^{-/-}$ mice were sacrificed and their femurs and tibias flushed with PBS using a 30G needle. Bone marrow cells were counted, resuspended to 1.0×10^6 cells/mL in macrophage medium [complete Iscove's modified Dulbecco's medium (IMDM) supplemented with 20 ng/mL M-CSF (315-02, PeproTech)], and incubated in nontissue culture–treated plates at 37°C for 1 week. Half the medium was replaced with fresh macrophage medium on day 4. Differentiated bone marrow–derived macrophages (BMDM) were polarized with 10 nmol/L dexamethasone for 24 hours, which induced Clever-1 expression in approximately 80% of wild-type macrophages. To detach macrophages, plates were washed with PBS and the cells incubated with 10 mmol/L EDTA in PBS.

Multiplex analyses

Blood from tumor-bearing mice was collected by cardiac puncture at endpoint. Serum samples were collected and stored at −70°C. Pieces weighing approximately 10 mg were cut from tumor edges, lysed in RIPA buffer (50 mmol/L Tris-HCl, 150 mmol/L NaCl, 1.0% Triton X-100, 0.5% sodium deoxycholate, 0.1% SDS) and stored at −70°C. Protein concentration was determined with the DC Protein Assay (5000111; Bio-Rad) and 10 μg of total protein was used for Multiplex. Enriched MDSCs and TAMs were plated at 0.5×10^6 cells/well in complete DMEM and stimulated with 0.1 μg/mL of LPS overnight. Supernatants were collected and stored at −70°C. To normalize multiplex readouts to cell number, the amount of DNA/well was determined with the CyQuant Kit (C35011; ThermoFisher Scientific). Multiplex analysis was performed with the Bio-Plex Pro Mouse Cytokine 23-plex assay (m60009rdpd; Bio-Rad) per the manufacturer's instructions. Samples were analyzed with the Bio-plex 200 system (Bio-Rad).

Seahorse assays

For the glycolysis stress test, enriched TAMs and MDSCs were plated at 0.1×10^6 cells/well in complete IMDM and left to adhere on Seahorse Assay Plates for 1 hour at 37°C. IMDM was replaced with Seahorse Assay Medium supplemented with 2 mmol/L L-glutamine. The cells were treated sequentially with 10 mmol/L glucose, 1 μmol/L oligomycin, and 50 mmol/L 2-deoxyglucose and analyzed with the Seahorse XF^e96 Extracellular Flux Analyzer (Agilent Technologies). For the metabolic phenotype test, wild-type and Clever-$1^{-/-}$ BMDMs were generated as described above and plated at 0.1×10^6 cells/well on Seahorse Assay Plates. IMDM was replaced with Seahorse Assay Medium supplemented with 10 mmol/L glucose, 2 mmol/L L-glutamine, and 1 mmol/L sodium pyruvate. The cells were treated with 1 μmol/L oligomycin and 1 μmol/L FCCP and analyzed as above. To normalize Seahorse Assay readouts to cell number, the amount of DNA/well was determined with the CyQuant Kit as above.

Quantitative PCR

Total RNA of dexamethasone-polarized and LPS-treated (50 ng/mL) BMDMs were isolated according to the manufacturer's instructions (NucleoSpin RNA; Macherey–Nagel). Five-hundred nanograms of extracted RNA was used as template for the reverse transcriptase reaction made with SuperScript VILO cDNA Synthesis Kit (Thermo Fisher Scientific). Roche Universal Library system was used for the quantitative PCR: 100 nmol/L of the UPL probes, 400 nmol/L of the primers (Clever-1: CTGTGTCCTGGTCCTCTGC and CGCAACGTTTAGACCGTACC, β-actin: CTAAGGCCAACCGTGAAAAG and ACCAGAGGCATACAGGGACA), and 5 ng of cDNA was used per well and three technical replicates were made. Reactions were run with QuantStudio 12K Flex Real-Time PCR System (Applied Biosystems/Thermo Fisher Scientific) at the Finnish Microarray and Sequencing Centre (FMSC), Turku Centre for Biotechnology, Turku, Finland. Relative expression of Clever-1 was calculated by using Sequence Detection System (SDS) Software v2.4.1, QuantStudio 12 K Flex software and DataAssist software (Applied Biosystems/Thermo Fisher Scientific). β-actin was used as an endogenous control.

Western blotting

Dexamethasone-polarized wild-type and Clever-1$^{-/-}$ BMDMs were stimulated with 50 ng/mL LPS for various time points and lysed with Triton X-100 lysis buffer (2% Triton X-100, 10 mmol/L Tris-HCl, 150 mmol/L NaCl, 1.5 mmol/L $MgCl_2$, 1 mmol/L phenylmethylsulfonyl fluoride, EDTA-free protease inhibitor cocktail). Protein concentration was measured with the Bradford method and equal amounts of protein (8–12 μg depending on the experiment) were loaded into 4% to 20% Mini-PROTEAN Precast Protein Gels (4561094; Bio-Rad). Separated proteins were transferred to membranes using a Trans-Blot Turbo Mini Nitrocellulose Transfer Pack (1704158; Bio-Rad). Membranes were incubated with primary antibodies against mouse p-mTOR S2248 (109368; Abcam), p-NF-κB S536 (3033S; Cell Signaling Technology), and GAPDH (5G4; Hytest Ltd.). IRDye 680RD donkey anti-mouse (C70419-09, LI-COR) and IRDye 800CW donkey anti-rabbit (C70918-02; LI-COR) were used as secondary antibodies. Fluorescence signal was detected with the Odyssey LI-COR Imaging System. Image analysis and band quantification were performed with ImageJ.

Statistical analyses

Data are presented as mean ± SEM with bar graphs additionally showing individual data points. Comparisons between groups were performed with the Mann–Whitney *U* test or the Kruskal–Wallis test followed by Mann–Whitney *U* tests. Comparisons between growth curves were performed with repeated measures two-way ANOVA followed by Tukey multiple comparisons tests. $P < 0.05$ was considered statistically significant. Statistical analyses were performed with Prism 7 (GraphPad).

Results

Macrophage Clever-1 deficiency significantly impairs tumor growth

To dissect the contribution of macrophage Clever-1 on the progression of solid tumors, we studied the outgrowth of subcutaneous LLC1 Lewis lung adenocarcinoma over 2 weeks in syngeneic wild-type, full Clever-1 knockout (Clever-1$^{-/-}$) and macrophage Clever-1 knockout (*Lyz2-Cre*/Clever-1$^{fl/fl}$) mice (10). The tumors grew comparably for the first week, after which tumor outgrowth was significantly impaired in Clever-1$^{-/-}$ and especially in *Lyz2-Cre*/Clever-1$^{fl/fl}$ mice (Fig. 1A and B; Supplementary Fig. S1A). Similarly, tumor weights were reduced in both Clever-1$^{-/-}$ and even more so in *Lyz2-Cre*/Clever-1$^{fl/fl}$ mice on day 15 (Fig. 1C). The increased tumor control in *Lyz2-Cre*/Clever-1$^{fl/fl}$ mice was also reflected in the substantial reduction of serum G-CSF, a cytokine produced by LLC1 tumors (Fig. 1D; ref. 21). In addition, tumors in both Clever-1$^{-/-}$ and *Lyz2-Cre*/Clever-1$^{fl/fl}$ mice contained significantly fewer nonhematopoietic tumor cells (gated on live CD45$^-$ cells; Fig. 1E; Supplementary Fig. S1B) with increased PD-L1 expression (Fig. 1F), suggesting that immunoediting of the surviving tumor cells occurred over the 2-week period. No significant difference was observed in the proliferation of tumor cells (Ki67$^+$) or the number of CD31$^+$ vascular endothelial cells on day 15 (Supplementary Fig. S1C).

As additional syngeneic cancer models, we studied the outgrowth of orthotopic E0771 medullary mammary adenocarcinoma and subcutaneous EL4 lymphoma in wild-type, Clever-1$^{-/-}$, and *Lyz2-Cre*/Clever-1$^{fl/fl}$ mice (Fig. 1G and H). Strikingly, the outgrowth of both E0771 and EL4 tumors was significantly impaired in *Lyz2-Cre*/Clever-1$^{fl/fl}$ mice, with all E0771 tumors cleared by day 15. However, neither cancer model showed clear reduction in tumor growth in Clever-1$^{-/-}$ mice (Fig. 1G and H). Still, the frequency of PD-L1$^+$ nonhematopoietic cells had increased also in E0771 tumors grown in Clever-1$^{-/-}$ mice (Supplementary Fig. S1D). In addition, the outgrowth of EL4 tumors was not impaired at all in *Tie2-Cre*/Clever-1$^{fl/fl}$ mice, where Clever-1 is deleted from the vascular endothelium (Fig. 1H), although anti-Clever-1 treatment of wild-type mice bearing EL4 tumors results in diminished size of primary tumors and metastases (10). Together, these results demonstrate that Clever-1 deficiency can significantly impair the progression of multiple syngeneic models of solid cancers. Furthermore, they suggest that the improved tumor control is mediated by macrophages but not by vascular endothelial cells deficient of Clever-1.

Clever-1–deficient mice can overcome cancer-related immunosuppression

LLC1 tumors are poorly immunogenic and induce general T-cell exhaustion, thus inhibiting antitumor immunity (22). To explore how Clever-1 deficiency affected the ongoing systemic immune responses in tumor-bearing wild-type, Clever-1$^{-/-}$, and *Lyz2-Cre*/Clever-1$^{fl/fl}$ mice, we analyzed serum cytokine levels on day 15. We found elevated levels of the key inflammatory cytokines IL1β, IL2, IL12p70, and TNFα as well as the inflammatory chemokines CCL3, CCL4, and CCL5 in Clever-1$^{-/-}$ mice, but surprisingly not so in *Lyz2-Cre*/Clever-1$^{fl/fl}$ mice (Fig. 2A and B). The lack of elevated cytokine levels in the serum of *Lyz2-Cre*/Clever-1$^{fl/fl}$ mice was probably consequent to their advanced tumor control. The observed increase in cytokines was tumor related because no differences were seen in nontumor-bearing mice between the genotypes apart from significantly higher IL1β in Clever-1$^{-/-}$ mice (data not shown).

We then investigated how Clever-1 deficiency affected adaptive immune activation in the TME. Immunofluorescence imaging of tumors collected from *Lyz2-Cre*/Clever-1$^{fl/fl}$ mice revealed massive infiltration of CD3$^+$ lymphocytes that were confirmed as CD8$^+$ T cells by flow cytometric analysis (pregated on live CD45$^+$ CD3$^+$ cells), although no significant differences in tumor-infiltrating lymphocytes were observed between tumors from wild-type and Clever-1$^{-/-}$ mice (Fig. 2C and D; Supplementary Fig. S2A). The amount of regulatory T cells (T_{reg}) (CD4$^+$ FoxP3$^+$) and CD4$^+$ T cells (CD4$^+$ FoxP3$^-$) were comparable between the genotypes (Fig. 2D). Still, the prognostic CD4$^+$/CD8$^+$ ratio decreased significantly in both Clever-1$^{-/-}$ and *Lyz2-Cre*/ Clever-1$^{fl/fl}$ mice (Fig. 2E). Moreover, the CD8$^+$ T cells in tumors from both Clever-1$^{-/-}$ and *Lyz2-Cre*/Clever-1$^{fl/fl}$ mice showed significantly increased coexpression of the exhaustion markers Lag3 and PD-1 (Fig. 2F) as did the CD4$^+$ T cells (Supplementary Fig. S2B), indicating robust and prolonged T-cell activation (23). In addition, we observed increased frequencies of proliferating CD8$^+$ effector T cells in the tumor-draining lymph nodes of Clever-1$^{-/-}$ and *Lyz2-Cre*/Clever-1$^{fl/fl}$ mice (Fig. 2G), suggesting that Clever-1 deficiency led to the increased priming of antitumor CD8$^+$ T cells outside the tumor.

Macrophages and CD8$^+$ T cells are required for tumor control in Clever-1–deficient mice

To validate that the strikingly improved tumor control in *Lyz2-Cre*/Clever-1$^{fl/fl}$ mice was not a nonspecific effect due to, for example, the Cre recombinase expressed under the *Lyz2* promoter,

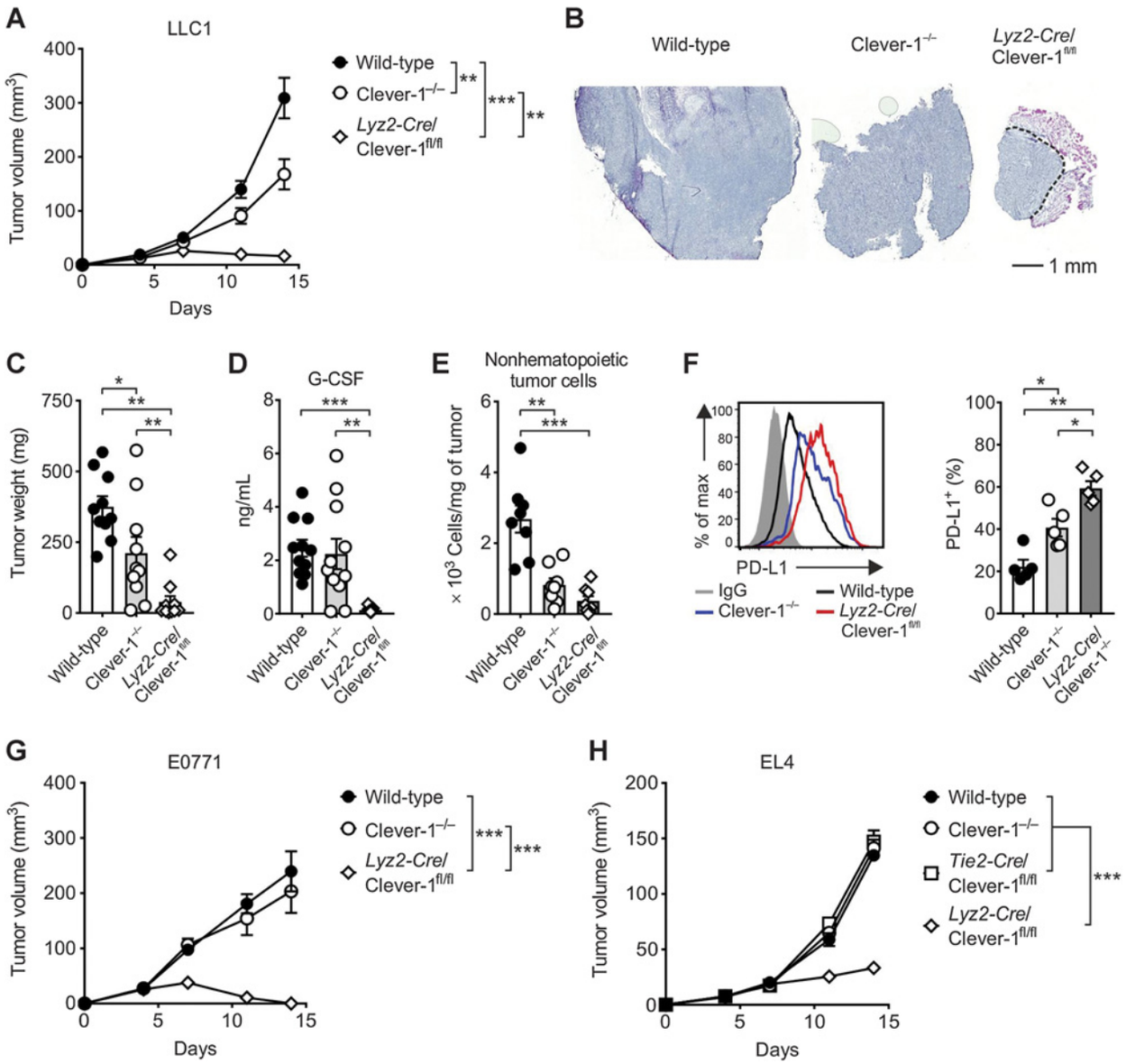

Figure 1.

Macrophage Clever-1 deficiency significantly impairs the progression of solid tumors. **A,** Outgrowth of subcutaneous LLC1 tumors in syngeneic wild-type, Clever-1$^{-/-}$, and *Lyz2-Cre*/Clever-1$^{fl/fl}$ mice. **B,** Representative hematoxylin/eosin-stained sections from LLC1 tumors collected on day 15. The dotted line demarcates the tumor mass and subcutaneous fat. Scale bar, 1 mm. **C,** Tumor weights, $n = 10$ per group. **D,** Serum concentrations of G-CSF in tumor-bearing mice, $n = 10$ per group. The data are combined from two independent experiments. **E,** Numbers of nonhematopoietic tumor cells (pregated on live CD45$^-$ cells) per mg of tumor, $n = 8$ mice per group. The data in **A**, **C**, and **E** are combined from three independent experiments. **F,** Representative histograms and frequencies of PD-L1$^+$ nonhematopoietic tumor cells, $n = 5$ per group. Gray, IgG control; black, wild type; blue, Clever-1$^{-/-}$; red, *Lyz2-Cre*/Clever-1$^{fl/fl}$. **G,** Outgrowth of orthotopic E0771 tumors in syngeneic female wild-type, Clever-1$^{-/-}$, and *Lyz2-Cre*/Clever-1$^{fl/fl}$ mice, $n = 5$ per group. **H,** Outgrowth of subcutaneous EL4 tumors in syngeneic wild-type, Clever-1$^{-/-}$, *Tie2-Cre*/ Clever-1$^{fl/fl}$, and *Lyz2-Cre*/ Clever-1$^{fl/fl}$ mice, $n = 5$ per group (*, $P < 0.05$; **, $P < 0.01$; *** $P < 0.001$).

we bred DsRed and DsRed/Clever-1$^{-/-}$ reporter mice and used them to create bone marrow chimeras to imitate the *Lyz2-Cre*/Clever-1$^{fl/fl}$ phenotype (Fig. 3A). Briefly, irradiated wild-type recipients were intravenously injected with bone marrow from DsRed or DsRed/Clever-1$^{-/-}$ donors and allowed to reconstitute for 2 months. Following reconstitution, we studied the outgrowth of LLC1 tumors in the resulting wild-type→wild-type and Clever-1$^{-/-}$→wild-type chimeras. Remarkably, tumor outgrowth was significantly impaired in the Clever-1$^{-/-}$→wild-type chimeras (Fig. 3B), with a concomitant increase in tumor-infiltrating CD8$^+$ T cells comparable with that observed in *Lyz2-Cre*/Clever-1$^{fl/fl}$ mice (Fig. 3C and D). TAMs in Clever-1$^{-/-}$→wild-type chimeras lacked Clever-1 expression and were decreased in frequency (Fig. 3C, E, and F). Furthermore, TAMs in Clever-1$^{-/-}$→wild-type chimeras expressed more MHC II and less CD206 (Fig. 3G and H), an established marker for M2

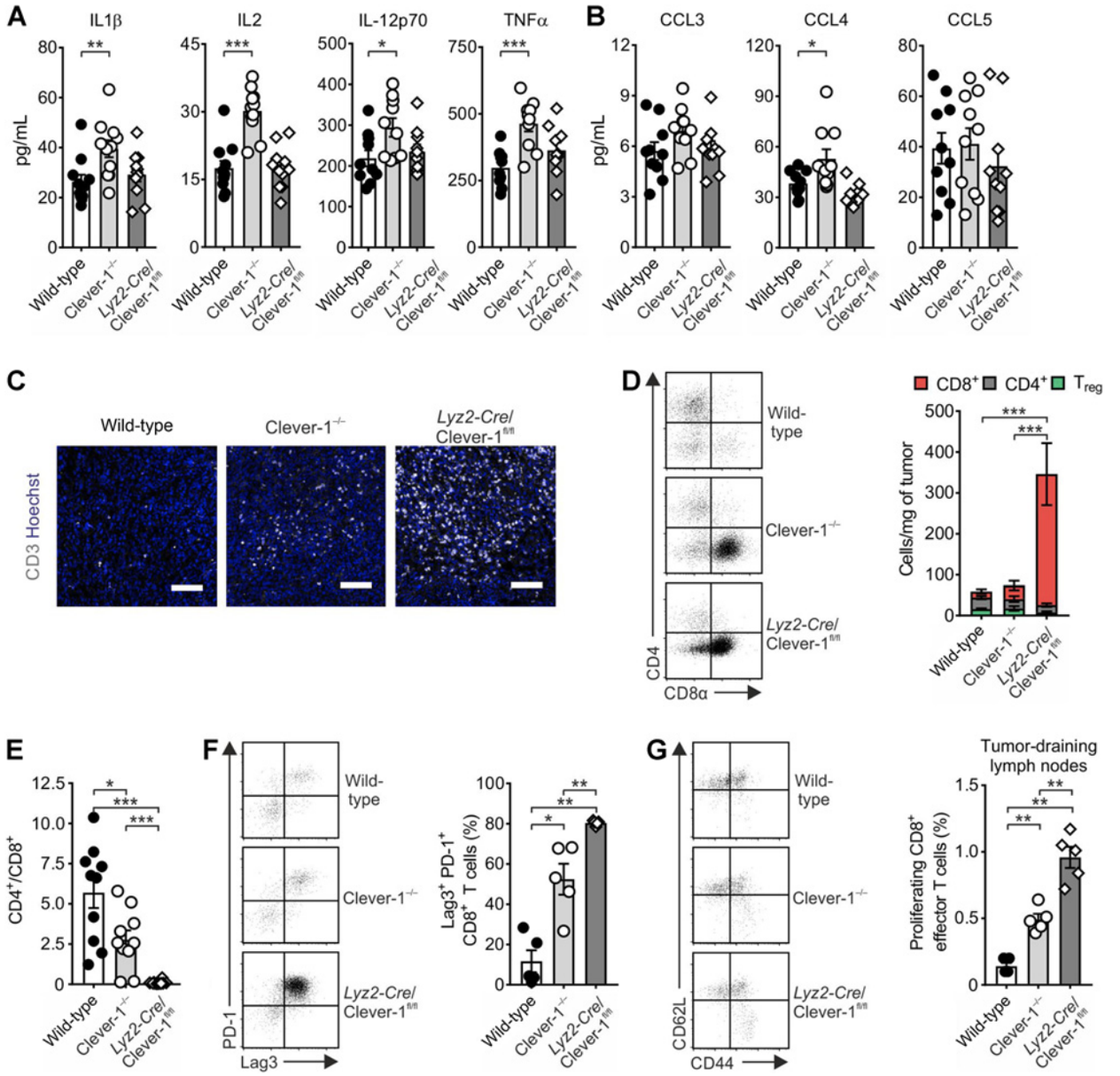

Figure 2.

Clever-1–deficient mice can overcome cancer-associated immunosuppression. **A** and **B,** Serum concentrations of the cytokines IL1β, IL2, IL12p70, and TNFα (**A**) and the chemokines CCL3, CCL4, and CCL5 (**B**) in mice bearing LLC1 tumors on day 15, $n = 10$ per group. The data are combined from two independent experiments. **C,** Representative immunofluorescence images showing tumor T-cell infiltration on day 8. Gray, CD3; blue, Hoechst stain. Scale bar, 100 μm. **D,** Representative dot plots and the number of T_{regs} ($CD4^+$ $CD8^-$ $FoxP3^+$), $CD4^+$ T cells ($CD4^+$ $CD8^-$ $FoxP3^-$), and $CD8^+$ T cells ($CD4^-$ $CD8^+$ $FoxP3^-$) (pregated on live $CD45^+$ $CD3^+$ cells) per mg of tumor on day 15. Statistical significances between $CD8^+$ T cells are shown; differences between other groups were not significant. **E,** Ratios of $CD4^+$ to $CD8^+$ T cells in tumors. The data in **D** and **E** are combined from three independent experiments, $n = 10$ per group. **F,** Representative dot plots and frequencies of $Lag3^+$ $PD\text{-}1^+$ $CD8^+$ T cells (pregated on live $CD45^+$ $CD3^+$ $CD8^+$ cells) as percentage of total tumor-infiltrating $CD8^+$ T cells, $n = 5$ per group. **G,** Representative dot plots and frequencies of proliferating $CD8^+$ effector T cells ($CD8^+$ $Ki67^+$ $CD44^{high}$ $CD62L^{low}$; pregated on live $CD45^+$ $CD3^+$ $CD8^+$ cells) in the tumor-draining lymph nodes of mice bearing LLC1 tumors, $n = 5$ per group (*, $P < 0.05$; **, $P < 0.01$; ***, $P < 0.001$).

macrophages. These results suggest that in the absence of macrophage Clever-1, TAMs acquire an immunostimulatory phenotype, which associates with increased tumor infiltration by $CD8^+$ T cells.

We then wanted to corroborate that macrophages are required to initiate tumor control in *Lyz2-Cre*/Clever-$1^{fl/fl}$ mice and to verify that this tumor control is executed by $CD8^+$ T cells. To this end, we depleted macrophages or $CD8^+$ T cells from wild-type and *Lyz2-Cre*/Clever-$1^{fl/fl}$ mice with antibodies against CD115 or CD8β, respectively, and measured the outgrowth of LLC1 tumors (Fig. 3I and J). Remarkably, depleting either macrophages or $CD8^+$ T cells reversed the efficient tumor control seen

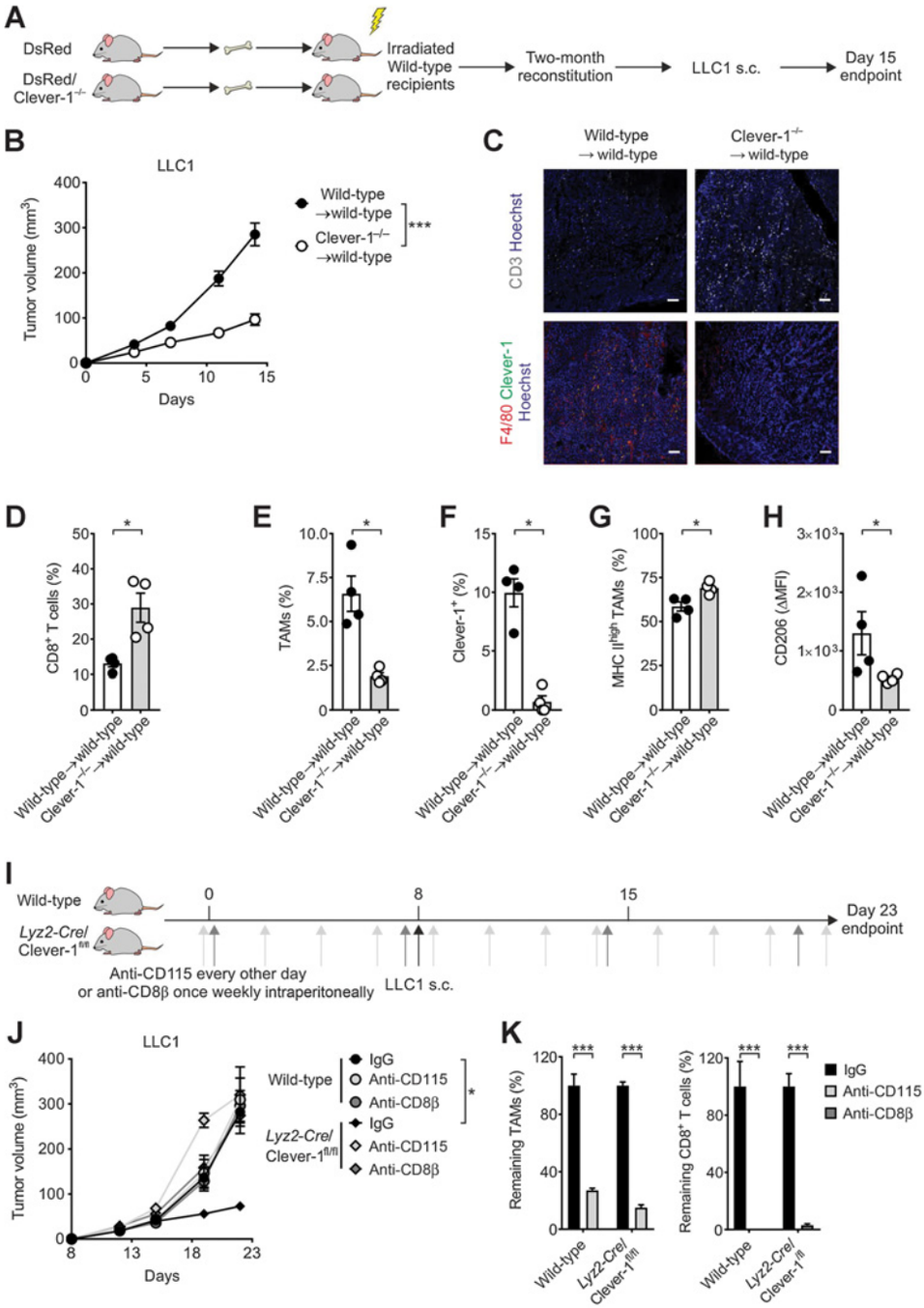

Figure 3.

Macrophages and CD8$^+$ T cells are essential for tumor control in Clever-1–deficient mice. **A,** Schematic study design for generating bone marrow chimeras by reconstituting lethally irradiated wild-type mice with bone marrow from DsRed or DsRed/Clever-1$^{-/-}$ mice and subsequent LLC1 cell injection. **B,** Outgrowth of LLC1 tumors in wild-type→wild-type and Clever-1$^{-/-}$→wild-type chimeras, $n = 8$ per group. **C,** Representative immunofluorescence images showing T-cell infiltration (top row) and TAMs and Clever-1 expression (bottom row) in LLC1 tumors on day 15. Top row: gray, CD3; blue, Hoechst stain. Bottom row: red, F4/80; green, Clever-1; blue, Hoechst stain. Scale bar, 100 μm. **D,** Frequencies of CD8$^+$ T cells (pregated on live CD45$^+$ CD3$^+$ cells) as percentage of total CD3$^+$ T cells, $n = 4$ mice per group. **E–G,** Frequencies of TAMs (gated on live CD11b$^+$ Ly6C^{low} Ly6G$^-$ MHC II$^+$ cells) as percentage of total cells (**E**) and Clever-1$^+$ TAMs (**F**) and MHC II^{high} TAMs (**G**) as percentage of total TAMs, $n = 4$ per group. **H,** Relative CD206 expression by TAMs, $n = 4$ per group. **I,** Schematic study design for depleting macrophages or CD8$^+$ T cells from wild-type and *Lyz2-Cre*/Clever-1$^{fl/fl}$ mice with anti-CD115 and anti-CD8β antibodies, respectively, before LLC1 cell injection. **J,** Outgrowth of subcutaneous LLC1 tumors in wild-type and *Lyz2-Cre*/Clever-1$^{fl/fl}$ mice treated with IgG, anti-CD115, or anti-CD8β antibodies. **K,** Remaining TAMs (left; gated on live CD45$^+$ CD3$^-$ CD8$^-$ CD11b$^+$ Ly6C^{low} Gr-1$^-$ cells) and CD8$^+$ T cells (right; gated on live CD45$^+$ CD3$^+$ CD8$^+$ CD11b$^-$ cells) as percentage of irrelevant IgG treatment. **J** and **K,** $n = 4$ per group +(*, $P < 0.05$; ***, $P < 0.001$).

in *Lyz2-Cre*/Clever-1$^{fl/fl}$ mice (Fig. 3J), demonstrating that Clever-1–deficient macrophages, in conjunction with CD8$^+$ T cells, are required to establish an efficient antitumor response. Flow cytometric analysis showed substantial depletion of TAMs and CD8$^+$ T cells from the TME at endpoint (Fig. 3K). Taken together, Clever-1–deficient macrophages are essential for initiating CD8$^+$ T-cell–mediated tumor control.

Clever-1 deficiency increases the immunostimulatory activity of TAMs

Our previous studies on the B16 mouse melanoma model suggested that much of the antitumor effect of Clever-1 deficiency would be mediated by the tumor endothelium (10). However, with the LLC1 lung cancer model, the improved tumor control in Clever-1–deficient mice became discernible approximately 1 week after cancer cell injection, at which point LLC1 tumors lacked Clever-1 expression on the endothelium but contained a high frequency of Clever-1$^+$ TAMs (Fig. 4A). At steady state, the frequency and distribution of macrophages (CD11b$^+$F4/80$^+$) in the blood, bone marrow, lungs, peripheral lymph nodes, and spleen of wild-type and Clever-1$^{-/-}$ mice was somewhat similar as we only observed roughly a 5% increase in bone marrow and a 5% decrease in blood macrophages in Clever-1$^{-/-}$ mice compared with wild-type mice (Supplementary Fig. S3A). By day 15, nearly all the tumor endothelial cells were Clever-1$^+$ (pregated on live CD45$^-$ CD31$^+$ cells), but little Clever-1 expression could be detected on CD45$^-$ CD31$^-$ tumor cells or CD45$^+$ CD11b$^+$ myeloid cells in the spleen or tumor-draining lymph nodes (Supplementary Fig. S3B). To investigate how Clever-1 deficiency could result in such efficient immune activation and tumor control, we analyzed the composition of the main myeloid cell populations (pregated on live CD11b$^+$ cells) found in tumors (Fig. 4B). Although the number of PMN-MDSCs (Ly6C^{intermediate} Ly6G$^+$) and M-MDSCs (Ly6C^{high} Ly6G$^-$) in LLC1 tumors were comparable between the genotypes, the number of TAMs (Ly6C^{low} Ly6G$^-$; pregated on live CD11b$^+$ cells; Supplementary Fig. S3C) were significantly reduced in Clever-1$^{-/-}$ mice and nearly absent from *Lyz2-Cre*/Clever-1$^{fl/fl}$ mice (Fig. 4B). On day 15, on average 30% of TAMs were Clever-1$^+$, and TAMs were the only myeloid cell population in tumors to express Clever-1 (Fig. 4C; Supplementary Fig. S3D). The majority of TAMs are the progeny of M-MDSCs that infiltrate the TME and polarize in response to environmental cues. Although tumors in Clever-1$^{-/-}$ mice contained fewer TAMs, M-MDSCs in tumors from Clever-1$^{-/-}$ mice actually expressed more Ki67 (Supplementary Fig. S3E), implying that the decrease in TAMs was not due to decreased M-MDSC infiltration or proliferation.

Although the number of total TAMs decreased in Clever-1$^{-/-}$ mice, the frequency of MHC II^{high} TAMs increased in tumors from Clever-1$^{-/-}$ mice (Fig. 4D). Intriguingly, the MHC II^{high} TAMs in Clever-1$^{-/-}$ mice coexpressed higher levels of CD206 (Fig. 4E). A similar phenotypic alteration was observed in TAMs from E0771 tumors collected from Clever-1$^{-/-}$ mice (Supplementary Fig. S3F). These differences were not due to increased numbers of dendritic cells, as tumors from Clever-1$^{-/-}$ mice actually contained fewer CD11c$^+$ MHC II^{high} cells (pregated on live cells; Supplementary Fig. S4A and S4B). Furthermore, TAMs from Clever-1$^{-/-}$ mice expressed less PD-L1 (Fig. 4F) and showed defective upregulation of inducible nitric oxide synthase (Nos2) after LPS stimulation *ex vivo* (Fig. 4G), whereas in PMN- and M-MDSCs, Nos2 expression was unaltered (Supplementary Fig. S5B). In addition, direct Multiplex analysis of tumor lysates showed increased IL12p40 in tumors from Clever-1$^{-/-}$ mice (Fig. 4H). Increased secretion of IL12p40 was detected also from the supernatants of enriched TAMs stimulated with LPS overnight (Fig. 4I), but not from MDSC supernatants (Supplementary Fig. S5A and S5C). Because of their scarcity, similar analyses could not be performed on TAMs from *Lyz2-Cre*/Clever-1$^{fl/fl}$ mice.

The increasingly inflammatory phenotype of Clever-1–deficient macrophages associates with increased mTOR activity

The immunostimulatory activation in TAMs associates with a metabolic switch from oxidative phosphorylation to glycolysis (24). To analyze metabolic differences between TAMs from wild-type and Clever-1$^{-/-}$ mice, we performed the Seahorse glucose stress test on enriched TAMs and observed increased glycolysis and glycolytic capacity (extracellular acidification rate, ECAR) in TAMs enriched from Clever-1$^{-/-}$ mice (Fig. 5A and B), whereas no difference in glycolytic activity was observed between MDSCs (Supplementary Fig. S5D and S5E). Typically, classically activated macrophages upregulate glycolytic pathways in response to increased mTOR activity (25). Thus, we investigated whether Clever-1 deficiency alters the activity of this inflammatory signaling pathway in BMDM derived from wild-type or Clever-1$^{-/-}$ mice. BMDMs were polarized with dexamethasone for 24 hours to induce robust Clever-1 expression (Supplementary Fig. S6A and S6B). In line with previous reports, Clever-1 deficiency did not inhibit macrophage differentiation *in vitro* (Supplementary Fig. S6C). However, flow cytometric analysis of dexamethasone-polarized BMDMs revealed a significant increase in the frequency of CD206$^+$ MHC II$^+$ double-positive cells in Clever-1$^{-/-}$ BMDM cultures (Fig. 5C), reflecting the phenotype of TAMs in Clever-1$^{-/-}$ mice. In addition, Clever-1$^{-/-}$ BMDMs expressed less PD-L1 on the cell surface (Fig. 5D) and secreted less IL10 after LPS stimulation (Fig. 5E).

Similar to Clever-1$^{-/-}$ TAMs, the dexamethasone polarized Clever-1$^{-/-}$ BMDMs showed increased glycolysis but not oxidative phosphorylation (oxygen consumption rate, OCR) at baseline (Fig. 5F and G). After overnight LPS stimulation, no differences were observed in the metabolic activity between wild-type and Clever-1$^{-/-}$ BMDMs (Fig. 5F and G). This was likely due to the rapid downregulation of Clever-1 mRNA in response to LPS (Fig. 5H). When the immediate responses to LPS stimulation were measured, Clever-1$^{-/-}$ BMDMs showed a rapid and prolonged increase in mTOR phosphorylation (Fig. 5I and J), which was corroborated also by flow cytometry (Fig. 5K) suggesting that metabolic remodeling was more efficient in the absence of Clever-1.

Immunotherapeutic Clever-1 blockade significantly impairs solid tumor growth

Previously, we have reported that immunotherapeutic Clever-1 blockade with the mStab1-1.26 antibody attenuates tumor growth in the B16 mouse melanoma model (10). To compare the effects of anti-Clever-1 treatment to an immunotherapeutic treatment mainly targeting the adaptive immune response, we treated mice bearing established LLC1 tumors with the anti-PD-1 antibody RMP1-14 (26) as monotherapy or in combination with anti-Clever-1 (Fig. 6A). All three treatments clearly reduced the size and weight of tumors compared with the irrelevant IgG treatment (Fig. 6B–D). Notably, tumors from

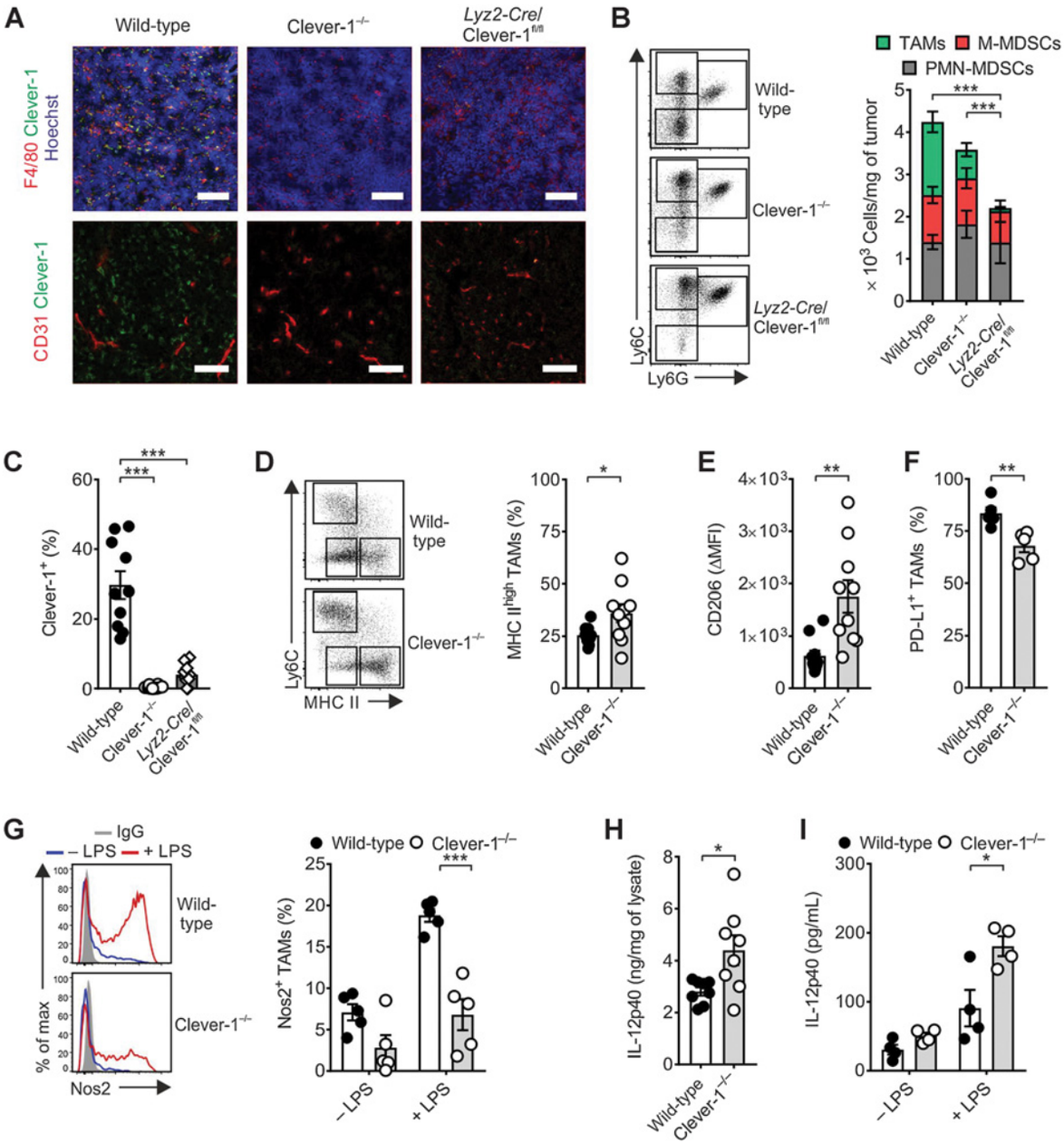

Figure 4.

TAMs acquire an immunostimulatory phenotype in the absence of Clever-1. **A,** Representative immunofluorescence images showing Clever-1 expression by TAMs (top row) and tumor endothelial cells (bottom row) in LLC1 tumors collected on day 8. Top row: red, F4/80; green, Clever-1; blue, Hoechst stain. Bottom row: red, CD31; green, Clever-1. Scale bar, 100 μm. **B,** Representative dot plots and amounts of TAMs (Ly6C^{low} Ly6G^{-} MHC II^{+}), M-MDSCs (Ly6C^{high} Ly6G^{-}), and PMN-MDSCs (Ly6C^{intermediate} Ly6G^{+}) (pregated on live CD11b^{+} cells) per mg of tumor on day 15. Statistical significances between TAMs are shown; differences between other groups were not significant. **C,** Relative Ki67 expression by M-MDSCs in tumors grown in wild-type and Clever-1$^{-/-}$ mice, $n = 5$ per group. **D,** Representative dot plots and frequencies of MHC II^{high} TAMs as percentage of total TAMs. **E,** Relative CD206 expression by MHC II^{high} TAMs. The data in **B–E** are combined from three independent experiments, $n = 10$ per group. **F,** Frequencies of PD-L1^{+} TAMs as percentage of total TAMs, $n = 5$ per group. **G,** Representative histograms and quantification of Nos2 induction in TAMs treated overnight with LPS, $n = 5$ per group. Gray, IgG control; blue, − LPS; red, + LPS. **H,** Concentration of IL12p40 in tumor lysates, $n = 8$ per group. **I,** Concentration of secreted IL12p40 in supernatants of TAMs isolated from tumors and stimulated with LPS overnight, $n = 4$ per group (*, $P < 0.05$; **, $P < 0.01$; ***, $P < 0.001$).

mice treated with anti-Clever-1 were even smaller than those treated with anti-PD-1, although the difference between the groups was not statistically significant. The combination treatment did not bring additional benefit to the monotherapies in the LLC1 model, and was accompanied by impaired clearance of nonhematopoietic tumor cells (Fig. 6E). To gain further

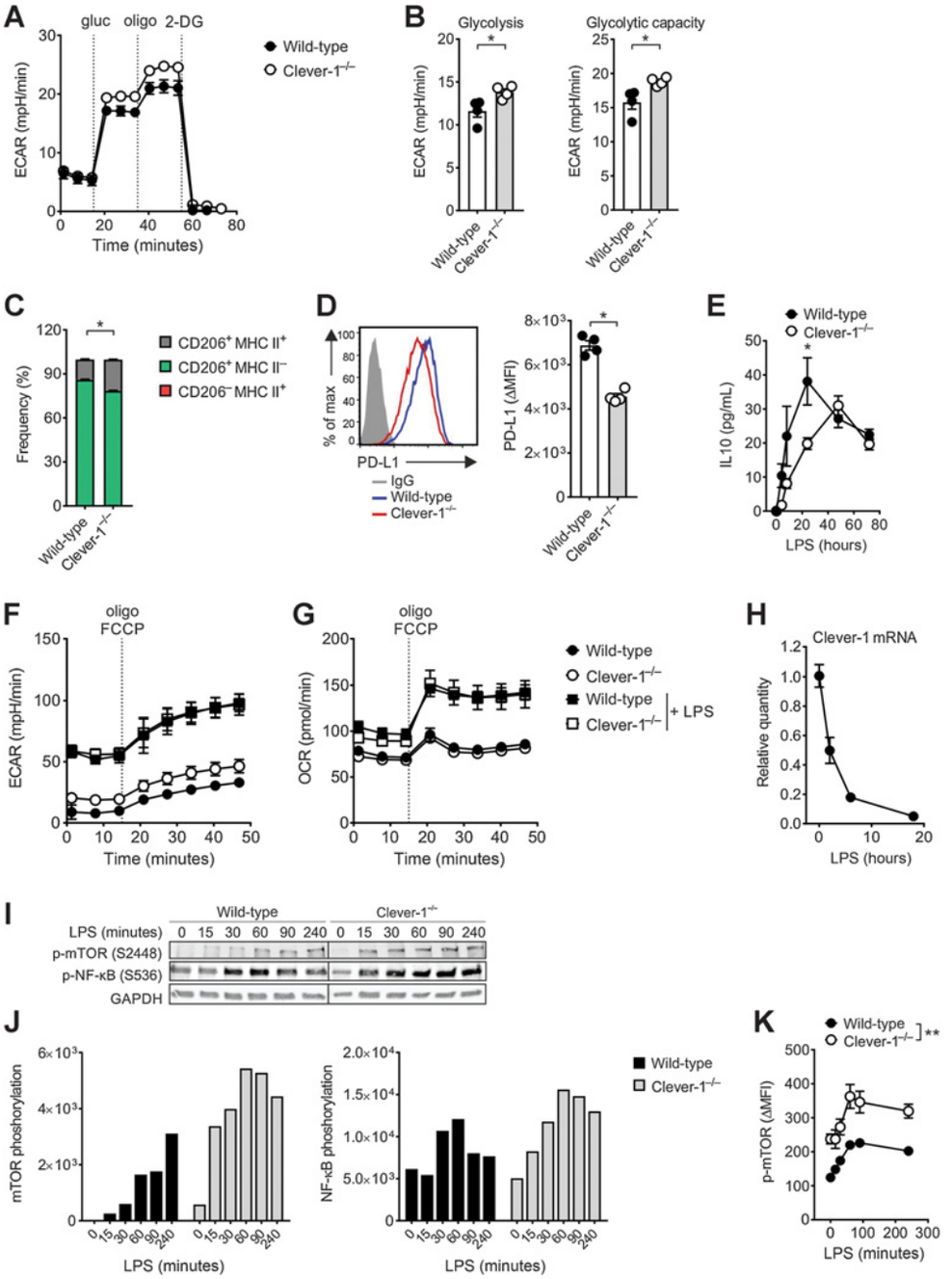

Figure 5.

Elevated mTOR signaling in Clever-1–deficient macrophages associates with an increasingly inflammatory phenotype. **A,** Glycolysis stress test on TAMs enriched from LLC1 tumors on day 15. Glucose (gluc), oligomycin (oligo), and 2-deoxyglucose (2-DG) were added at the indicated time points. ECAR, extracellular acidification rate. **B,** Quantified glycolysis (left) and glycolytic capacity (right) in TAMs. **A** and **B**, $n = 4$ per group. **C,** Frequencies of CD206$^+$ MHC II$^+$, CD206$^+$ MHC II$^-$, and CD206$^-$ MHC II$^-$ wild-type and Clever-1$^{-/-}$ BMDMs after polarization with dexamethasone. **D,** Relative PD-L1 expression by dexamethasone-polarized wild-type and Clever-1$^{-/-}$ BMDMs. **E,** IL10 secretion by dexamethasone-polarized wild-type and Clever-1$^{-/-}$ BMDMs after LPS stimulation. **C**–**E**, $n = 4$ per group. **F** and **G,** Metabolic phenotype test showing glycolysis (**F**) and oxidative phosphorylation (**G**) on dexamethasone-polarized wild-type and Clever-1$^{-/-}$ BMDMs at baseline and after LPS stimulation overnight (+ LPS). Oligomycin (oligo) and FCCP were added at the indicated time points. OCR, oxygen consumption rate. **H,** Relative Clever-1 mRNA expression in dexamethasone-polarized wild-type BMDMs after LPS stimulation, $n = 3$. **I,** Representative Western blots showing mTOR and NF-κB phosphorylation after LPS stimulation in dexamethasone-polarized wild-type and Clever-1$^{-/-}$ BMDMs. GAPDH serves as the loading control. The experiment was repeated five times with similar results. **J,** Band quantification of mTOR (left) and NF-κB (right) phosphorylation in **I** normalized to GAPDH. **K,** Relative mTOR phosphorylation in dexamethasone-polarized wild-type and Clever-1$^{-/-}$ BMDMs after LPS stimulation analyzed by flow cytometry, $n = 4$ per group (*, $P < 0.05$; **, $P < 0.01$).

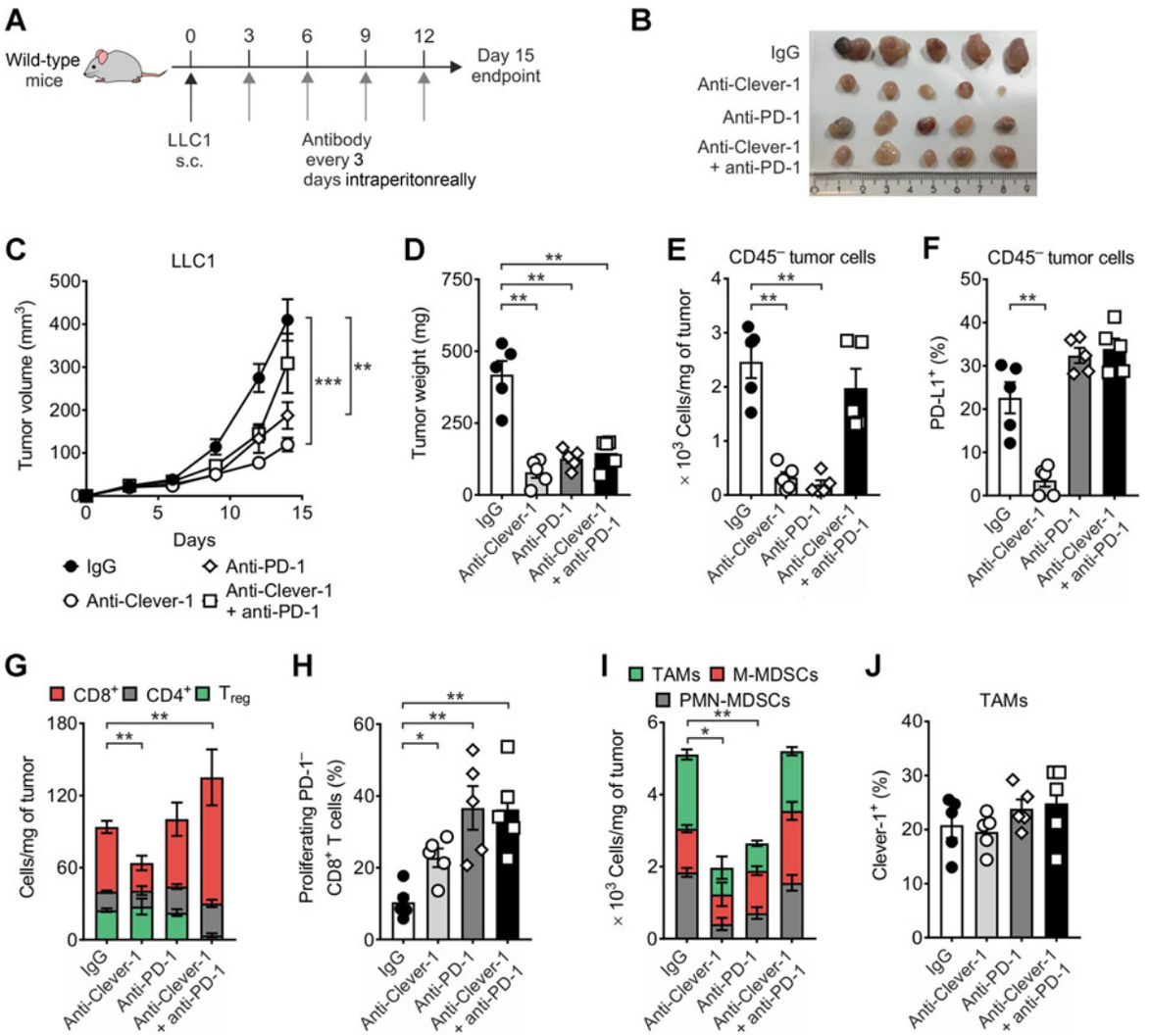

Figure 6.

Immunotherapeutic Clever-1 blockade significantly limits tumor growth and reactivates the antitumor CD8$^+$ T-cell response. **A,** Schematic study design for treating tumor-bearing wild-type mice with antibodies against Clever-1, PD-1, or combination thereof. **B,** Photograph of tumors collected on day 15. **C,** Outgrowth of LLC1 tumors in wild-type mice treated as indicated in **A**. **D,** Tumor weights. **E,** Numbers of nonhematopoietic tumor cells (gated on live CD45$^-$ cells) per mg of tumor. **F,** Frequencies of PD-L1$^+$ nonhematopoietic tumor cells as percentage of total nonhematopoietic tumor cells. **G,** Numbers of T_{regs} (CD4$^+$ CD8$^-$ FoxP3$^+$), CD4$^+$ T cells (CD4$^+$ CD8$^-$ FoxP3$^-$), and CD8$^+$ T cells (CD4$^-$ CD8$^+$ FoxP3$^-$) (pregated on live CD45$^+$ CD3$^+$ cells) per mg of tumor. Statistical significance between CD8$^+$ T cells is shown; other differences were not significant. **H,** Frequencies of proliferating PD-1$^-$ CD8$^+$ T cells (Ki67$^+$ PD-1$^-$ CD8$^+$; pregated on live CD45$^+$ CD3$^+$ CD8$^+$ cells) as percentage of total tumor-infiltrating CD8$^+$ T cells. **I,** Numbers of TAMs (Ly6C^{low} Ly6G$^-$ MHC II$^+$), M-MDSCs (Ly6C^{high} Ly6G$^-$), and PMN-MDSCs (Ly6C^{intermediate} Ly6G$^+$) (pregated on live CD11b$^+$ cells) per mg of tumor. The shown statistical significances refer to differences between TAMs and PMN-MDSCs; differences between M-MDSCs were not significant. **J,** Frequencies of Clever-1$^+$ TAMs as percentage of total TAMs. **B–J,** $n = 5$ per group (*, $P < 0.05$; **, $P < 0.01$; ***, $P < 0.001$).

insight into the mechanisms of tumor rejection mediated by Clever-1 interference, the treatment regimens were repeated with the metastasizing 4T1-luc2 breast cancer and immunogenic CT26.WT colon carcinoma models (27). The combination of anti-Clever-1 and anti-PD-1 was most effective at inhibiting 4T1-luc2 tumor growth, viability, and metastasis to the lungs and tumor-draining lymph nodes (Supplementary Fig. S7A–S7D). Also, in the CT26.WT model, the combination treatment brought slightly more effect compared with anti-PD-1 alone (Supplementary Fig. S7E–S7G). Interestingly, only anti-Clever-1 treatment led to a decrease in the frequencies of PD-L1$^+$ nonhematopoietic tumor cells in the immunologically cold LLC1 model (Fig. 6F), suggesting that anti-PD-1 treatment induces immunotherapeutic resistance mediated by the upregulation of PD-L1, but that this mechanism may not be protective against Clever-1 blockade alone. Conversely, in the immunologically hot CT26.WT model, wherein a much higher frequency of tumor cells were PD-L1$^+$ to start with, the combinatorial treatment most successfully decreased the frequencies of PD-L1$^+$ tumor cells (Supplementary Fig. S7H).

Clever-1 antibody blockade reactivates the antitumor CD8$^+$ T-cell response

When analyzing the adaptive immune response, we did not observe any significant differences in the numbers of tumor-infiltrating CD4$^+$ T cells or T_{regs} between the treatments (Fig. 6G). Surprisingly, however, we observed that the numbers of CD8$^+$ T cells were actually decreased in LLC1 tumors treated with anti-Clever-1 alone (Fig. 6G), but the frequencies of tumor-infiltrating CD4$^+$ effector T cells (CD44^{high} CD62L^{low}) and CD8$^+$ memory T cells (CD44^{high} CD62L^{high}) were significantly increased in tumors treated with anti-Clever-1, even more so compared with Clever-1$^{-/-}$ mice (Supplementary Fig. S8A and S8B). Furthermore, the numbers of CD8$^+$ T cells were unchanged in tumors treated with anti-PD-1 alone and significantly increased in tumors treated with the combination (Fig. 6G). Despite these differences, all three treatments increased the frequencies of proliferating PD-1$^-$ CD8$^+$ T cells (Fig. 6H), implicating that both anti-Clever-1 and anti-PD-1 treatment can reactivate antitumor CD8$^+$ T cells and that these treatments can work synergistically in this regard. Interestingly, although the total TAM and PMN-MDSC populations were greatly reduced by anti-Clever-1 and anti-PD-1 treatments alone, their combination normalized the distribution of tumor-associated myeloid cells to that of irrelevant IgG treatment (Fig. 6I), thus perhaps explaining the impairment in tumor cell clearance. The frequencies of Clever-1$^+$ TAMs remained unaltered in all three treatments (Fig. 6J), suggesting that the observed effects were not caused by the depletion of Clever-1$^+$ TAMs. Surface staining with the directly conjugated mStab1-1.26 antibody showed that virtually all Clever-1 on TAMs was occupied following antibody treatment (Supplementary Fig. S8C). Curiously, in CT26.WT tumors, only anti-PD-1 treatment increased the numbers of CD8$^+$ T cells and the frequencies of proliferating PD-1$^-$ CD8$^+$ T cells, although the combination of anti-Clever-1 and anti-PD-1 retained their levels comparable with those of the irrelevant IgG treatment (Supplementary Fig. S7I and S7J). In CT26.WT tumors, anti-Clever-1 treatment alone significantly reduced the numbers of both M-MDSCs and TAMs, and the treatment with anti-PD-1 significantly reduced the numbers of TAMs (Supplementary Fig. S7K). Although the combination of anti-Clever-1 and anti-PD-1 somewhat normalized the distribution of tumor-associated myeloid cells in CT26.WT tumors similarly to what was observed in the LLC1 tumors, the numbers of TAMs remained significantly reduced in comparison with the irrelevant IgG treatment (Supplementary Fig. S7K). In addition, it resulted in a slight reduction in Clever-1$^+$ TAMs (Supplementary Fig. S7L). Taken together, these results demonstrate that anti-Clever-1 treatment results in similar adaptive immune activation in the TME as genetic Clever-1 deficiency, and that these effects are comparable to what can be achieved with PD-1 checkpoint blockade.

Discussion

Because of the recent successes but emerging shortcomings in immunotherapy, novel treatment strategies that activate the antitumor immune response are a topic of major interest in cancer immunology research. In this study, we show a significant function of the scavenger receptor Clever-1 in controlling macrophage-mediated local and systemic antitumor immune responses. Our data support Clever-1 targeting as a novel approach to increase host defense against immunocompromised tumors alongside PD-1 blockade. Exceptionally, the improved tumor control in our study was achieved by targeting the innate arm of immunity, which undoubtedly underlines the importance of macrophages in controlling the fate of tumor-reactive T cells. This is also supported by the notion that macrophage-targeted approaches are needed to achieve full immunotherapeutic efficacy (28, 29). Importantly, Advani and colleagues report substantial antitumor responses in non-Hodgkin lymphoma by blocking the CD47-SIRPα checkpoint together with anti-CD20, suggesting that macrophage-mediated antibody-dependent tumor cell phagocytosis can be complementary to activating T-cell–mediated tumor killing (30, 31).

Recent studies highlight the importance of DCs in the activation of antitumor immunity (32–34). Although DCs are reportedly more efficient at T-cell priming than TAMs, macrophages can also prime CD8$^+$ T cells to generate cytotoxic effector cells and CD8$^+$ T-cell memory *in vivo* (32, 35). Moreover, tumorigenic TAMs are extremely potent immunosuppressors both individually and through sheer numbers (32, 36, 37). For example, tumor-infiltrating CD8$^+$ T cells mostly come into contact with TAMs because of their high frequency, and TAMs can directly induce CD8$^+$ T-cell apoptosis and physically restrict CD8$^+$ T cells from reaching their target cells 39 ,38 ,32)).

Paradoxically, complete TAM depletion with CSF-1R inhibition has not yielded therapeutic benefits as monotherapy, and more effective responses have been reached by combining it with chemotherapy, adoptive cell transfer, or checkpoint blockade (40–43). In comparison, monotherapies aimed at repolarizing TAMs have presented more promising results (44–46). A possible reason for this is that some TAM populations susceptible to CSF-1R depletion are needed for efficient antitumor control. This is in line with our data showing that the effective tumor control gained by blocking Clever-1 on TAMs is fully abolished by CSF-1R treatment. It is interesting to note that although Clever-1 is used as a common marker for alternatively activated macrophages, it is only expressed by 20% to 40% of TAMs in various mouse tumor models. Despite their relatively low numbers, our data suggest that Clever-1 expression defines a subpopulation of TAMs capable of limiting effective antitumor immune responses. In fact, blocking Clever-1 skewed TAMs toward an immunostimulatory phenotype with increased MHC II expression and IL12p40 secretion, thus enabling efficient antigen presentation and improving tumor control by boosting infiltration of CD8$^+$ T cells, respectively (47). Similarly, Clever-1 knockdown in human monocytes increases their ability to reactivate T cells in antigen recall assays (11). Intriguingly, the aforementioned changes were accompanied by increased CD206 expression by MHC II^{high} TAMs. Although CD206 is an established marker for alternatively activated macrophages and mostly associated with a negative impact on tumor control, macrophages have been shown to use CD206 for endocytosing soluble antigens for cross-presentation and CD8$^+$ T-cell activation (48, 49). We did not observe a similar mixed TAM phenotype in the Clever-1$^{-/-}$ bone marrow chimeras, indicating that compensatory mechanisms contributing to the loss of Clever-1 on endothelial cells might have induced CD206 expression on MHC II^{high} TAMs. Similarly, the PD-L1 induction on cancer cells in the conditional and full knockout mice was not recapitulated after immunotherapeutic Clever-1 blockade, again pointing to compensatory mechanisms that might have developed during the lifespan of these mice.

However, the induction of Nos2 was impaired in Clever-1$^{-/-}$ TAMs in response to *ex vivo* LPS stimulation. As Nos2 is greatly induced by classical activation (50), our observations were not in line with a general view of the functional traits seen in classically activated macrophages, *per se*. However, the TME contains multitudes of danger-associated molecular patterns that can prime and activate TAMs. We can speculate that differences in the composition of the TME, created either by active tumor lysis or the impaired scavenging of extracellular matrix components due to the loss of Clever-1, modify the secondary responses of TAMs to nonrelated stimuli, in this case to LPS. Along these lines, human monocytes primed with β-glucan downregulate ROS production when restimulated with LPS but upregulate it when primed with either the bacillus Calmette-Guérin (BCG) vaccine or oxidized low-density lipoprotein (oxLDL; ref. 51). Overall, excessive nitric oxide production by Nos2 has been shown to suppress classical activation, interfere with antigen recognition, and induce T-cell apoptosis (38, 52–54).

The priming of macrophages induces a metabolic switch from oxidative phosphorylation to glycolysis. Consistent with the priming hypothesis, Clever-1$^{-/-}$ TAMs demonstrated increased glycolysis, suggesting that effective priming had occurred within the TME of LLC1 tumors in the absence of Clever-1. The mTOR signaling network orchestrates a multitude of cellular and metabolic activities that shape immune effector responses. In mice, increased mTORC1 activity and reduced mTORC2 activity by ablation of *Tsc1* has been shown to promote M1 macrophage polarization (25). The increased glycolysis in Clever-1$^{-/-}$ TAMs was in line with the observed increase in phosphorylation of mTOR in Clever-1$^{-/-}$ BMDMs after LPS stimulation. Because the mTOR complex is localized within endosomes, it can be speculated that mechanistically Clever-1 attenuates mTOR activity by regulating its endosomal trafficking. In support of this, the intracellular part of Clever-1 contains a GGA-binding site that is required for intracellular sorting of its ligands (55). Furthermore, a recent report shows that the adaptation of metabolism after LPS stimulation in macrophages mainly occurs through proteome remodeling at the translational level (56), and therefore might explain why Clever-1 deficiency has not been reported to induce major transcriptional changes in TAMs (17).

One apparent difference was seen in the impaired ability of Clever-1 full knockout mice to mount equally effective tumor rejection in comparison to mice lacking Clever-1 expression only on macrophages, despite similar but milder antitumor responses. Most likely the reason can be attributed to endothelial Clever-1, which has been reported to mediate immune cell adhesion to the tumor endothelium (10) as well as support immune and cancer cell migration through blood and lymphatic vessels (12, 14, 16, 57–59). As we detected here, Clever-1 is induced in TAMs earlier than on the tumor endothelium and increased infiltration of T cells in tumors occurred before endothelial Clever-1 expression. Although the kinetics of Clever-1 expression may differ between cancer models, it is possible that tumor endothelial Clever-1 is required to maintain CD8$^+$ T-cell infiltration at later time points. Also, the contribution of lymphatic endothelial Clever-1 to immune responses remains to be clarified, as it may facilitate cell migration through lymph vessels into the tumor-draining lymph nodes. Therefore, we believe that the loss of Clever-1 on lymphatic or vascular endothelium in Clever-1$^{-/-}$ mice impairs the infiltration of activated lymphocyte subsets in the TME and therefore counteracts to the proinflammatory effects produced by Clever-1–deficient TAMs in *Lyz2-Cre*/Clever-1$^{fl/fl}$ mice (Supplementary Fig. S8D).

The antitumor effects obtained by immunotherapeutic Clever-1 blockade with the mStab1 antibody were paradoxically more similar to the *Lyz2-Cre*/Clever-1$^{fl/fl}$ mice than the Clever-1$^{-/-}$ mice. Because Clever-1 is a very large scavenger receptor (∼280 kDa) and has several functional binding sites for its ligands, the binding of mStab1 on Clever-1 may not fully block the amino acid residues that lymphocytes use for their adhesion to the tumor endothelium but sufficiently block macrophage scavenging. Rantakari and colleagues demonstrate that the human Clever-1 antibody 3-372 can revert LDL scavenging related suppression of CCL3 secretion by human monocytes (19). We observed a similar increase in CCL3 secretion in mStab1-treated mouse macrophages (data not shown), and therefore believe that macrophage conversion is achieved with the mStab1 antibody. Intriguingly, our unpublished observations (Tadayon and colleagues, resubmitted after revisions) indicate that Clever-1 can bind to the surface of both B and CD8$^+$ T cells, suggesting that Clever-1 could inhibit these cells directly by an unknown ligand, and complementing the immunosuppressive nature it has on TAMs.

Importantly, immunotherapeutic Clever-1 blockade showed a significant therapeutic effect in LLC1 tumors, which was comparable or even slightly more robust than the effect seen with anti-PD-1. Both of these immunotherapies altered tumor-infiltrating immune cell populations in a similar manner, resulting in decreased numbers of TAMs and PMN-MDSCs and increased frequencies of activated CD8$^+$ T cells. The lower abundance of TAMs and PMN-MDSCs can partially explain the therapeutic effect. However, the frequency of Clever-1$^+$ TAMs did not change after anti-Clever-1 treatment, suggesting that the effect does not come from the depletion of Clever-1$^+$ cells due to antibody-dependent cell cytotoxicity. Curiously, the numbers of total CD8$^+$ T cells were decreased by anti-Clever-1 treatment. This may be a result of endothelial Clever-1 blockade, as the numbers of total CD8$^+$ T cells were not increased in Clever-1$^{-/-}$ mice either. A noteworthy dissimilarity between anti-Clever-1 and anti-PD-1 treatments was the downregulation of PD-L1 on nonimmune tumor cells after treatment with anti-Clever-1 but not anti-PD-1. This suggests that upregulation of the PD-L1 checkpoint, a common mechanism of immunotherapeutic resistance, is not protective against anti-Clever-1 treatment, or that alternative resistance mechanisms are activated by anti-Clever-1 treatment.

The therapeutic effect of anti-Clever-1 treatment in different tumor types might not be directly reflected to the number of Clever-1$^+$ TAMs in the TME. The immunologically cold LLC1 tumors contained half the number of Clever-1$^+$ TAMs compared with the CT26.WT tumors and yet produced much higher response rates as monotherapy. One possible reason for this is the high expression of PD-L1 on CT26.WT cells that was not downregulated by anti-Clever-1 monotherapy in a similar fashion as seen in LLC1 tumors. Lack of PD-L1 expression on malignant cells has been shown to delay tumor growth in a CD8$^+$ T-cell-mediated fashion (60). Thus, despite higher numbers of CD8$^+$ T cells in the combination-treated LLC1 tumors, consistent PD-L1 expression on LLC1 cells might have rendered this combination ineffective. However, the combination treatment in the CT26.WT model significantly suppressed PD-L1 expression on the tumor

cells and produced a modest synergistic effect compared with anti-PD-1 alone.

Taken together, we propose that the improved tumor control is specifically a result of macrophage Clever-1 deficiency, which increases the frequency of immunostimulatory TAMs while reducing their total numbers, together rendering the TME more permissive to $CD8^+$ T-cell activation. In addition, we show that immunotherapeutic anti-Clever-1 treatment can achieve comparable outcomes to PD-1 checkpoint blockade, strongly supporting the clinical evaluation of Clever-1 targeting as a novel cancer treatment strategy.

Disclosure of Potential Conflicts of Interest

S. Jalkanen holds ownership interest (including patents) in Faron Pharmaceuticals. M. Hollmén reports receiving other commercial research support from, is a consultant/advisory board member for, and holds ownership interest (including patents) in Faron Pharmaceuticals. No potential conflicts of interest were disclosed by the other authors.

Authors' Contributions

Conception and design: M. Viitala, R. Virtakoivu, S. Tadayon, S. Jalkanen, M. Hollmén

Development of methodology: M. Viitala, R. Virtakoivu, S. Tadayon, M. Hollmén

Acquisition of data (provided animals, acquired and managed patients, provided facilities, etc.): M. Viitala, R. Virtakoivu, S. Tadayon, J. Rannikko, M. Hollmén

Analysis and interpretation of data (e.g., statistical analysis, biostatistics, computational analysis): M. Viitala, R. Virtakoivu, S. Tadayon, J. Rannikko, M. Hollmén

Writing, review, and/or revision of the manuscript: M. Viitala, R. Virtakoivu, S. Jalkanen, M. Hollmén

Administrative, technical, or material support (i.e., reporting or organizing data, constructing databases): M. Viitala, R. Virtakoivu, M. Hollmén

Study supervision: S. Jalkanen, M. Hollmén

Acknowledgments

The authors thank M. Parsama, S. Mäki, T. Kanasuo, and R. Sjöroos for excellent technical assistance. The authors thank the Cell Imaging Core at the Turku Centre for Biotechnology and the Central Animal Laboratory at the University of Turku for their expertise and service. This study was financially supported by the Sigrid Jusélius Foundation (to M. Hollmén), the Finnish Academy (to M. Hollmén and S. Jalkanen), the Finnish Cancer Foundation (to S. Jalkanen), and the Finnish Cultural Foundation (to R. Virtakoivu).

The costs of publication of this article were defrayed in part by the payment of page charges. This article must therefore be hereby marked *advertisement* in accordance with 18 U.S.C. Section 1734 solely to indicate this fact.

Received September 13, 2018; revised January 8, 2019; accepted February 6, 2019; published first February 12, 2019.

References

1. Zou W, Wolchok JD, Chen L. PD-L1 (B7-H1) and PD-1 pathway blockade for cancer therapy: mechanisms, response biomarkers, and combinations. Sci Transl Med 2016;8:328rv4.
2. Chen Daniel S, Mellman I. Oncology meets immunology: the cancer–immunity cycle. Immunity 2013;39:1–10.
3. Gajewski TF, Schreiber H, Fu Y-X. Innate and adaptive immune cells in the tumor microenvironment. Nat Immunol 2013;14:1014–22.
4. Chen DS, Mellman I. Elements of cancer immunity and the cancer–immune set point. Nature 2017;541:321–30.
5. Sharma P, Hu-Lieskovan S, Wargo JA, Ribas A. Primary, adaptive, and acquired resistance to cancer immunotherapy. Cell 2017;168:707–23.
6. Mantovani A, Marchesi F, Malesci A, Laghi L, Allavena P. Tumour-associated macrophages as treatment targets in oncology. Nat Rev Clin Oncol 2017;14:399–416.
7. Kzhyshkowska J, Gratchev A, Goerdt S. Stabilin-1, a homeostatic scavenger receptor with multiple functions. J Cell Mol Med 2006;10:635–49.
8. Ammar A, Mohammed RA, Salmi M, Pepper M, Paish EC, Ellis IO, et al. Lymphatic expression of CLEVER-1 in breast cancer and its relationship with lymph node metastasis. Anal Cell Pathol 2011;34:67–78.
9. Algars A, Irjala H, Vaittinen S, Huhtinen H, Sundström J, Salmi M, et al. Type and location of tumor-infiltrating macrophages and lymphatic vessels predict survival of colorectal cancer patients. Int J Cancer 2012;131:864–73.
10. Karikoski M, Marttila-Ichihara F, Elima K, Rantakari P, Hollmen M, Kelkka T, et al. Clever-1/stabilin-1 controls cancer growth and metastasis. Clin Cancer Res 2014;20:6452–64.
11. Palani S, Elima K, Ekholm E, Jalkanen S, Salmi M. Monocyte stabilin-1 suppresses the activation of Th1 lymphocytes. J Immunol 2016;196:115–23.
12. Irjala H, Alanen K, Grenman R, Heikkila P, Joensuu H, Jalkanen S. Mannose receptor (MR) and common lymphatic endothelial and vascular endothelial receptor (CLEVER)-1 direct the binding of cancer cells to the lymph vessel endothelium. Cancer Res 2003;63:4671–6.
13. Kzhyshkowska J, Gratchev A, Schmuttermaier C, Brundiers H, Krusell L, Mamidi S, et al. Alternatively activated macrophages regulate extracellular levels of the hormone placental lactogen via receptor-mediated uptake and transcytosis. J Immunol 2008;180:3028–37.
14. Karikoski M, Irjala H, Maksimow M, Miiluniemi M, Granfors K, Hernesniemi S, et al. Clever-1/Stabilin-1 regulates lymphocyte migration within lymphatics and leukocyte entrance to sites of inflammation. Eur J Immunol 2009;39:3477–87.
15. Park SY, Jung MY, Lee SJ, Kang KB, Gratchev A, Riabov V, et al. Stabilin-1 mediates phosphatidylserine-dependent clearance of cell corpses in alternatively activated macrophages. J Cell Sci 2009;122:3365–73.
16. Shetty S, Weston CJ, Oo YH, Westerlund N, Stamataki Z, Youster J, et al. Common lymphatic endothelial and vascular endothelial receptor-1 mediates the transmigration of regulatory T cells across human hepatic sinusoidal endothelium. J Immunol 2011;186:4147–55.
17. Riabov V, Yin S, Song B, Avdic A, Schledzewski K, Ovsiy I, et al. Stabilin-1 is expressed in human breast cancer and supports tumor growth in mammary adenocarcinoma mouse model. Oncotarget 2016;7:31097–110.
18. Palani S, Maksimow M, Miiluniemi M, Auvinen K, Jalkanen S, Salmi M. Stabilin-1/CLEVER-1, a type 2 macrophage marker, is an adhesion and scavenging molecule on human placental macrophages. Eur J Immunol 2011;41:2052–63.
19. Rantakari P, Patten DA, Valtonen J, Karikoski M, Gerke H, Dawes H, et al. Stabilin-1 expression defines a subset of macrophages that mediate tissue homeostasis and prevent fibrosis in chronic liver injury. Proc Natl Acad Sci U S A 2016;113:9298–303.
20. Schledzewski K, Falkowski M, Moldenhauer G, Metharom P, Kzhyshkowska J, Ganss R, et al. Lymphatic endothelium-specific hyaluronan receptor LYVE-1 is expressed by stabilin-1+, F4/80+, CD11b+ macrophages in malignant tumours and wound healing tissue in vivo and in bone marrow cultures in vitro: implications for the assessment of lymphangiogenesis. J Pathol 2006;209:67–77.
21. Shojaei F, Wu X, Qu X, Kowanetz M, Yu L, Tan M, et al. G-CSF-initiated myeloid cell mobilization and angiogenesis mediate tumor refractoriness to anti-VEGF therapy in mouse models. Proc Natl Acad Sci U S A 2009;106:6742–7.
22. Mittal R, Chen CW, Lyons JD, Margoles LM, Liang Z, Coopersmith CM, et al. Murine lung cancer induces generalized T cell exhaustion. J Surg Res 2015;195:541–9.
23. Woo SR, Turnis ME, Goldberg MV, Bankoti J, Selby M, Nirschl CJ, et al. Immune inhibitory molecules LAG-3 and PD-1 synergistically regulate T cell function to promote tumoral immune escape. Cancer Res 2012;72:917–27.
24. Kelly B, O'Neill LA. Metabolic reprogramming in macrophages and dendritic cells in innate immunity. Cell Res 2015;25:771–84.

25. Byles V, Covarrubias AJ, Ben-Sahra I, Lamming DW, Sabatini DM, Manning BD, et al. The TSC-mTOR pathway regulates macrophage polarization. Nat Commun 2013;4:2834.
26. Chen S, Lee LF, Fisher TS, Jessen B, Elliott M, Evering W, et al. Combination of 4-1BB agonist and PD-1 antagonist promotes antitumor effector/memory CD8 T cells in a poorly immunogenic tumor model. Cancer Immunol Res 2015;3:149–60.
27. Lechner MG, Karimi SS, Barry-Holson K, Angell TE, Murphy KA, Church CH, et al. Immunogenicity of murine solid tumor models as a defining feature of in vivo behavior and response to immunotherapy. J Immunother 2013;36:477–89.
28. Fridlender ZG, Jassar A, Mishalian I, Wang L-C, Kapoor V, Cheng G, et al. Using macrophage activation to augment immunotherapy of established tumours. Br J Cancer 2013;108:1288.
29. Van der Sluis TC, Sluijter M, van Duikeren S, West BL, Melief CJM, Arens R, et al. Therapeutic peptide vaccine-induced CD8 T cells strongly modulate intratumoral macrophages required for tumor regression. Cancer Immunol Res 2015;3:1042–51.
30. Advani R, Flinn I, Popplewell L, Forero A, Bartlett NL, Ghosh N, et al. CD47 blockade by Hu5F9-G4 and rituximab in non-Hodgkin's lymphoma. N Engl J Med 2018;379:1711–21.
31. Mantovani A, Longo DL. Macrophage checkpoint blockade in cancer - back to the future. N Engl J Med 2018;379:1777–9.
32. Broz ML, Binnewies M, Boldajipour B, Nelson AE, Pollack JL, Erle DJ, et al. Dissecting the tumor myeloid compartment reveals rare activating antigen-presenting cells critical for T cell immunity. Cancer Cell 2014;26:638–52.
33. Roberts EW, Broz ML, Binnewies M, Headley MB, Nelson AE, Wolf DM, et al. Critical role for CD103+/CD141+ dendritic cells bearing CCR7 for tumor antigen trafficking and priming of T cell immunity in melanoma. Cancer Cell 2017;30:324–36.
34. Spranger S, Dai D, Horton B, Gajewski TF. Tumor-residing Batf3 dendritic cells are required for effector T cell trafficking and adoptive T cell therapy. Cancer Cell 2017;31:711–23.
35. Pozzi L-AM, Maciaszek JW, Rock KL. Both dendritic cells and macrophages can stimulate naïve CD8+ T cells in vivo to proliferate, develop effector function, and differentiate into memory cells. J Immunol 2005;175:2071–81.
36. Kusmartsev S, Gabrilovich DI. STAT1 signaling regulates tumor-associated macrophage-mediated T cell deletion. J Immunol 2005;174:4880–91.
37. Hamilton MJ, Bosiljcic M, LePard NE, Halvorsen EC, Ho VW, Banáth JP, et al. Macrophages are more potent immune suppressors ex vivo than immature myeloid-derived suppressor cells induced by metastatic murine mammary carcinomas. J Immunol 2014;192:512–22.
38. Saio M, Radoja S, Marino M, Frey AB. Tumor-infiltrating macrophages induce apoptosis in activated CD8+ T cells by a mechanism requiring cell contact and mediated by both the cell-associated form of TNF and nitric oxide. J Immunol 2001;167:5583–93.
39. Peranzoni E, Lemoine J, Vimeux L, Feuillet V, Barrin S, Kantari-Mimoun C, et al. Macrophages impede CD8+ T cells from reaching tumor cells and limit the efficacy of anti-PD-1 treatment. Proc Natl Acad Sci U S A 2018;115:E4041–E50.
40. DeNardo DG, Brennan DJ, Rexhepaj E, Ruffell B, Shiao SL, Madden SF, et al. Leukocyte complexity predicts breast cancer survival and functionally regulates response to chemotherapy. Cancer Discov 2011;1:54–67.
41. Mok S, Koya RC, Tsui C, Xu J, Robert L, Wu L, et al. Inhibition of CSF-1 receptor improves the antitumor efficacy of adoptive cell transfer immunotherapy. Cancer Res 2014;74:153–61.
42. Zhu Y, Knolhoff BL, Meyer MA, Nywening TM, West BL, Luo J, et al. CSF1/CSF1R blockade reprograms tumor-infiltrating macrophages and improves response to T cell checkpoint immunotherapy in pancreatic cancer models. Cancer Res 2014;74:5057–69.
43. Cannarile MA, Weisser M, Jacob W, Jegg A-M, Ries CH, Rüttinger D. Colony-stimulating factor 1 receptor (CSF1R) inhibitors in cancer therapy. J Immunother Cancer 2017;5:53.
44. Lum HD, Buhtoiarov IN, Schmidt BE, Berke G, Paulnock DM, Sondel PM, et al. Tumoristatic effects of anti-CD40 mAb-activated macrophages involve nitric oxide and tumour necrosis factor-α. Immunology 2006;118:261–70.
45. Georgoudaki AM, Prokopec KE, Boura VF, Hellqvist E, Sohn S, Ostling J, et al. Reprogramming tumor-associated macrophages by antibody targeting inhibits cancer progression and metastasis. Cell Rep 2016;15:2000–11.
46. Kaneda MM, Messer KS, Ralainirina N, Li H, Leem CJ, Gorjestani S, et al. PI3Kγ is a molecular switch that controls immune suppression. Nature 2016;539:437.
47. Kanemaru H, Yamane F, Fukushima K, Matsuki T, Kawasaki T, Ebina I, et al. Antitumor effect of Batf2 through IL-12p40 up-regulation in tumor-associated macrophages. Proc Natl Acad Sci U S A 2017;114:7331–40.
48. Burgdorf S, Lukacs-Kornek V, Kurts C. The mannose receptor mediates uptake of soluble but not of cell-associated antigen for cross-presentation. J Immunol 2006;176:6770–6.
49. Burgdorf S, Kautz A, Böhnert V, Knolle PA, Kurts C. Distinct Ppathways of antigen uptake and intracellular routing in CD4+ and CD8+ T cell activation. Science 2007;316:612–6.
50. Biswas SK, Allavena P, Mantovani A. Tumor-associated macrophages: functional diversity, clinical significance, and open questions. Semin Immunopathol 2013;35:585–600.
51. Bekkering S, Blok BA, Joosten LA, Riksen NP, van Crevel R, Netea MG. In vitro experimental model of trained innate immunity in human primary monocytes. Clin Vaccine Immunol 2016;23:926–33.
52. Nagaraj S, Gupta K, Pisarev V, Kinarsky L, Sherman S, Kang L, et al. Altered recognition of antigen is a mechanism of CD8+ T cell tolerance in cancer. Nat Med 2007;13:828.
53. Lu T, Ramakrishnan R, Altiok S, Youn J-I, Cheng P, Celis E, et al. Tumor-infiltrating myeloid cells induce tumor cell resistance to cytotoxic T cells in mice. J Clin Invest 2011;121:4015–29.
54. Lu G, Zhang R, Geng S, Peng L, Jayaraman P, Chen C, et al. Myeloid cell-derived inducible nitric oxide synthase suppresses M1 macrophage polarization. Nat Commun 2015;6:6676.
55. Kzhyshkowska J, Gratchev A, Martens JH, Pervushina O, Mamidi S, Johansson S, et al. Stabilin-1 localizes to endosomes and the trans-Golgi network in human macrophages and interacts with GGA adaptors. J Leukoc Biol 2004;76:1151–61.
56. Jovanovic M, Rooney MS, Mertins P, Przybylski D, Chevrier N, Satija R, et al. Immunogenetics. Dynamic profiling of the protein life cycle in response to pathogens. Science 2015;347:1259038.
57. Irjala H, Elima K, Johansson EL, Merinen M, Kontula K, Alanen K, et al. The same endothelial receptor controls lymphocyte traffic both in vascular and lymphatic vessels. Eur J Immunol 2003;33:815–24.
58. Qian H, Johansson S, McCourt P, Smedsrod B, Ekblom M. Stabilins are expressed in bone marrow sinusoidal endothelial cells and mediate scavenging and cell adhesive functions. Biochem Biophys Res Commun 2009;390:883–6.
59. Boström MM, Irjala H, Mirtti T, Taimen P, Kauko T, Algars A, et al. Tumor-associated macrophages provide significant prognostic information in urothelial bladder cancer. PLoS One 2015;10:e0133552.
60. Kleinovink JW, Marijt KA, Schoonderwoerd MJA, van Hall T, Ossendorp F, Fransen MF. PD-L1 expression on malignant cells is no prerequisite for checkpoint therapy. Oncoimmunology 2017;6:e1294299.